International Journal of Biological Macromolecules 49 (2011) 871–878

Contents lists available at ScienceDirect

International Journal of Biological Macromolecules

journal homepage: www.elsevier.com/locate/ijbiomac

# Thermal unfolding of apo- and holo-enolase from *Saccharomyces cerevisiae*: Different mechanisms, similar activation enthalpies

Liliana M. Moreno-Vargas, Normandé Carrillo-Ibarra, Lilian Arzeta-Pino, Claudia G. Benítez-Cardoza*

*Laboratorio de Investigación Bioquímica, Programa Institucional en Biomedicina Molecular, ENMyH-Instituto Politécnico Nacional, D.F., Mexico*

ARTICLE INFO

*Article history:*
Received 8 June 2011
Received in revised form 24 July 2011
Accepted 28 July 2011
Available online 4 August 2011

*Keywords:*
Thermal unfolding kinetics
Intermediate state
Monomer
Dimer
Circular dichroism
Irreversibility
Molten globule
Cofactor

ABSTRACT

Yeast enolase is stabilized by its natural cofactor $Mg^{2+}$. This stabilization is ascribed to the reduced subunit dissociation of the holoprotein. Nevertheless, how $Mg^{2+}$ alters the unfolding mechanism has yet to be fully characterized. Here, we investigate the role of $Mg^{2+}$ in the denaturation mechanism and unfolding kinetics of yeast enolase. Apo-enolase unfolds through a three-state process ($N_2 \leftrightarrow 2I \rightarrow 2D$). The intermediate species is described as a monomeric molten globule-like conformation that becomes noticeable in the presence of phosphate and is able to recover its native secondary structure when cooled down. Kinetic studies confirmed the presence of the intermediate species, even though it was not noticeable in the thermal scans. The cofactor increases the cooperativity of the unfolding transitions, while the intermediate species becomes less noticeable or nonexistent. Thus, holo-enolase follows a simple two-state mechanism ($N_2 \rightarrow 2D$). Our results indicate smaller unfolding rate-constants in the presence of $Mg^{2+}$, thus favoring the native state. The temperature dependence of the unfolding rates allowed us to calculate the activation enthalpies of denaturation. Interestingly, despite the different unfolding mechanisms of the apo and holo forms of enolase, they both have similar activation barriers of denaturation (185–190 kJ $mol^{-1}$).



## 1. Introduction

Enolase (2-phosphoglycerate hydrolyase, E.C. 4.2.1.11) is a multifunctional (moonlighting) protein that plays important roles in several biological and pathophysiological processes. It has been identified as a heat-shock protein [1] and as a plasminogen receptor on the cell surface of a variety of hematopoietic, endothelial and epithelial cells [2,3]. It can also bind to cytoskeletal and chromatin structures, and some studies have detected anti-enolase antibodies in a variety of autoimmune diseases [4]. Thus, its expression varies according to the pathophysiological, metabolic or developmental conditions of the cell [5]. In addition, enolase catalyzes the reversible dehydration of 2-phosphoglycerate to form phosphoenol pyruvate, requiring two moles of divalent metal cations per subunit for this task [6,7]. $Mg^{2+}$ is the physiological cofactor of enolase and promotes its highest activity, but some other metals like $Mn^{2+}$ and $Zn^{2+}$ can also bind and activate the enzyme, whereas $Ca^{2+}$, $Ba^{2+}$, $Sr^{2+}$, $Hg^{2+}$, $Pb^{2+}$, and $Be^{2+}$ can bind enolase but are not capable of activating the enzyme. When $Mg^{2+}$ first binds to a subunit, it facilitates the binding of a substrate/product that in turn enables a second $Mg^{2+}$ to bind, and catalysis can thus proceed [8]. One $Mg^{2+}$ atom interacts with the carboxylate-oxygen atoms of Asp246, Asp320, and Glu295, as well as the carboxylate of the substrate/product. The second $Mg^{2+}$ atom forms a bridge with the oxygen atoms of Ser39 as well as with the oxygen atoms from the carboxylate and phosphate groups of the substrate/product [9–15]. Some reports indicate that $Mg^{2+}$ concentrations over 1 mM inhibit catalysis, probably due to a reduction in the rate of product release [16]. Structurally, enolase is a dimeric protein where each monomer has a large domain (C-terminal) with an $\alpha\alpha\beta\beta(\alpha\beta)_6$ barrel folding-type and a small domain (N-terminal) with 3 $\alpha$-helices and 4 $\beta$-sheets. Both domains include loops that fold over the active site when the substrate is bound. Most of the intersubunit contacts are between the small domain of one monomer and the large domain of the other [11,17–20].

Some reports indicate that heat induces the dissociation of yeast enolase [21]. Others suggest that the binding of substrate or analogs, as well as di- or trivalent cations, increases its thermal stability, probably by inducing the closure of the loops near the active site, which could result in a more highly packed protein. It has also been suggested that the binding of divalent cations increases thermal stability by reducing subunit dissociation. This could imply that dissociation might occur before denaturation without a divalent

*Abbreviations:* CD, circular dichroism; tris, tris(hydroxy-methyl) aminomethane; Gdn-HCl, guanidine hydrochloride; PGA, 2-phosphoglycerate; PEP, phosphoenolpyruvate.

* Corresponding author at: Laboratorio de Investigación Bioquímica, Sección de Estudios de Posgrado, ENMyH-IPN, Guillermo Massieu Helguera No. 239, La Escalera Ticoman, D.F. 07320, Mexico. Tel.: +52 55 57296300x55562.
*E-mail address:* beni1972uk@gmail.com (C.G. Benítez-Cardoza).

0141-8130/$ – see front matter © 2011 Elsevier B.V. All rights reserved.
doi:10.1016/j.ijbiomac.2011.07.021

cation, but there is no clear experimental evidence to support this statement [22]. Some other studies have analyzed the effect of several mutations in yeast enolase. In most cases, mutations decrease the temperature stability, as well as the susceptibility to proteolytic digestion [9,15,23]. For these reasons, the aim of this study was to analyze the thermal stability, as well as the folding/unfolding mechanism of yeast enolase, and particularly the role of $Mg^{2+}$ in the folding pathway, which remains to be thoroughly understood. We studied the temperature–induced denaturation of enolase under a wide range of experimental conditions, using circular dichroism (CD), as well as fluorescence spectroscopy, to monitor the thermodynamics and kinetics of enolase structural transitions. Our results indicate that the apo and holo forms of yeast enolase unfold through different mechanisms with similar kinetic barriers.

## 2. Materials and methods

### 2.1. Materials

Yeast enolase was purchased from Sigma and was used without any further purification. Homogeneity of the sample was verified by SDS-PAGE. Protein concentrations were estimated spectrophotometrically at 280 nm, with an extinction coefficient reported for enolase of $\varepsilon = 0.895\ mg\ mL^{-1}$ [42]. Most experiments were carried out using enolase solutions prepared at a concentration of $0.010\ mg\ mL^{-1}$, but some were performed using concentrations ranging from 0.010 to $0.100\ mg\ mL^{-1}$, as stated. In addition, studies were carried out in three different buffers: tris–acetate, tris–HCl, or potassium phosphate (each at 50 mM, pH 7.4), as stated. In some experiments, solutions were complemented with 2 mM $MgSO_4$, 2 mM $MgCl_2$, or 1 mM EDTA as indicated. All reagents were of analytical grade, and the water used was distilled and deionized. In all cases, curves are reported as the average of at least two independent experiments. All assays were made using the same protein batch, but to verify the data, experiments were repeated using a different protein batch.

### 2.2. Enolase activity assays

The enolase activity was measured by coupling its reaction to pyruvate kinase and lactate dehydrogenase and following the decrease of NADH absorbance at 340 nm using a Beckman DU-650 spectrophotometer. This assay was performed at 25 °C in a 0.1 mL reaction mixture containing 0.05 M of potassium phosphate, tris–acetate, or tris–HCl buffer, pH 7.4, 1.9 mM PGA, 1.3 mM ADP, 0.12 mM NADH, 25 μM $MgSO_4$, and 10 mM KCl. Auxiliary enzymes were used at final activities of 2.3 and $3.3\ U\ mL^{-1}$. One activity unit is defined as the conversion of 1.0 μmol of PGA to PEP per minute [24].

### 2.3. Fluorescence

Fluorescence experiments were carried out using the JASCO J-815 CD spectropolarimeter equipped with a FMO-427 emission monochromator for fluorescence detection accessory, and a PFD-425S Peltier temperature controller. The sample was contained in a 1.0-cm quartz cuvette. All experiments were obtained using 1.0-cm path length cells. The excitation wavelength was 280 nm, and the emission spectra were collected from 320 to 400 nm.

### 2.4. Thermal transitions monitored by circular dichroism spectroscopy

CD measurements were performed in a JASCO J-815 spectropolarimeter (Jasco Inc., Easton, MD), equipped with a PFD-425S Peltier-type cell holder for temperature control and magnetic stirring. CD spectra were recorded from 200 to 250 nm, using 1.0-cm path-length cells. Ellipticities are reported as the mean residue ellipticity [$\theta$]. Thermal denaturation transitions were followed by continuously monitoring ellipticity changes at a fixed wavelength of 220 nm, while the temperature of the sample was increased at a constant heating rate, usually $2\ °C\ min^{-1}$, or as stated in the text. Actual temperatures within the cell were registered with the external cell holder probe. Cooling profiles were recorded after denaturation transitions had been completed. Both heating and cooling profiles were controlled through the Peltier accessory.

### 2.5. Denaturation kinetics

The kinetic curves of yeast enolase denaturation were obtained by monitoring changes in ellipticity at 220 nm or fluorescence emission (excitation and emission wavelengths were 280 and 340 nm, respectively). The 1.0 cm-path length cells were filled up to 98% of their total volume (3.0 mL) with tris–acetate buffer for equilibration at the temperature of the experiment, which was measured with the external probe of the Peltier accessory. After this, we injected the necessary amount of concentrated enolase solution to complete the cell volume. Samples were vigorously stirred to promote rapid mixing and temperature equilibration. Under these conditions, the setup time of the experiments was less than 10 s. Kinetic data were adjusted to single ($\theta t = \theta f + A\ exp[-kt]$) or double exponential decay equations ($\theta t = \theta f + A1\ exp[-k_1 t] + A2\ exp[-k_2 t]$), accordingly; where $\theta t$ is the signal measured at time $t$, $\theta f$ is the final signal value, $A$, $A_1$ and $A_2$ represent amplitudes of each phase, and, $k$, $k_1$ and $k_2$ are the unfolding rate constants for each reaction.

### 2.6. 1-Anilino-8-naphthalene sulfonate (ANS) fluorescence

Binding of the hydrophobic dye ANS was measured by fluorescence spectroscopy. The excitation wavelength was 380 nm, and emission was collected at 497 nm. ANS was used under saturating concentrations (100 μM). The procedure to start the kinetic experiments was similar to the one described for circular dichroism and intrinsic fluorescence.

## 3. Results

We have previously demonstrated that the secondary and tertiary structures of native yeast enolase do not undergo important modifications due to a change in buffers, as judged by superposable circular dichroism and fluorescence spectra. Furthermore, activity assays indicated the same specific activity ($110\ U\ mg^{-1}$) for enolase in tris–acetate or tris–HCl buffers, whereas it decreased ($70\ U\ mg^{-1}$) when using phosphate buffer, which was as expected because phosphate is a competitive inhibitor of enolase [24].

### 3.1. Yeast enolase thermal denaturation transitions

Yeast enolase temperature-induced denaturation profiles in potassium phosphate, tris–HCl or tris–acetate buffers, containing 1 mM EDTA, were followed by monitoring ellipticity at 220 nm, with constant heating-rates ($2\ °C\ min^{-1}$), shown in Fig. 1. We observed that transitions obtained in tris–acetate and tris–HCl without $Mg^{2+}$ appear as single sigmoidal curves, being more cooperative in tris–acetate, whereas the transition in phosphate buffer without $Mg^{2+}$ appears as a bimodal sigmoidal curve, indicating the presence of at least one possible intermediate species between 52 and 56 °C.

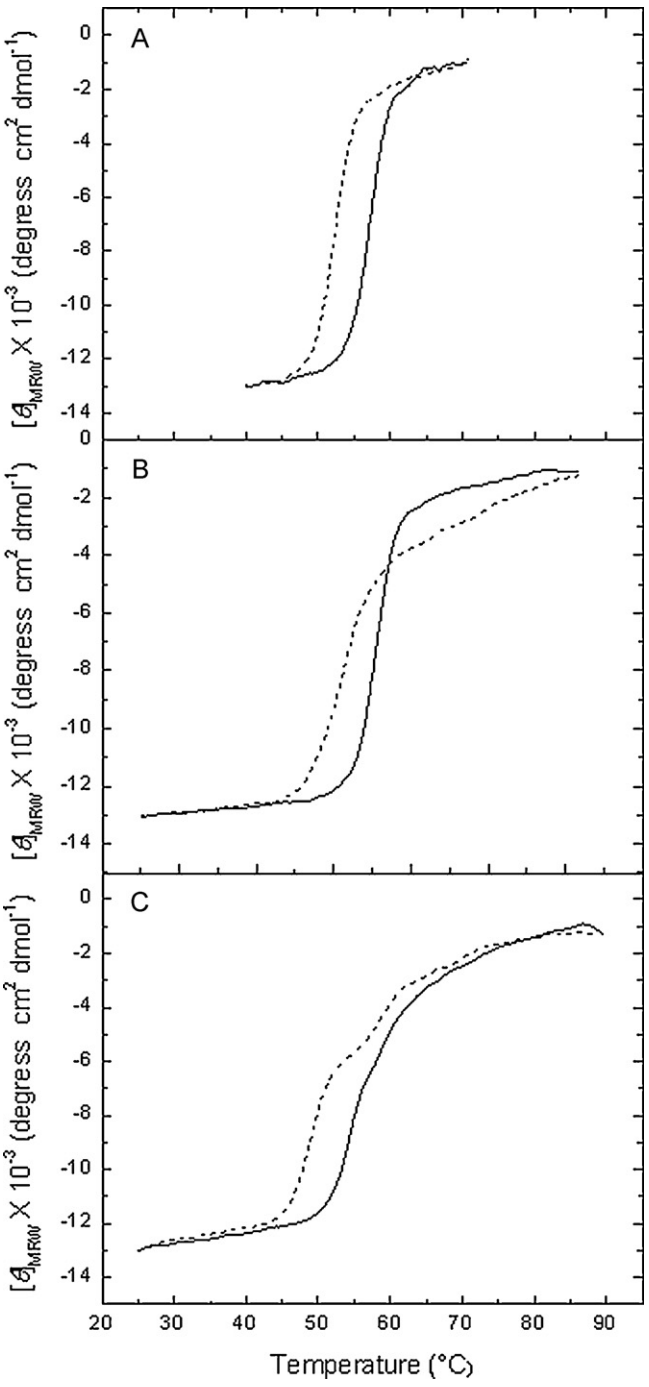


**Fig. 1.** Temperature-induced denaturation profiles of yeast enolase monitored by circular dichroism spectroscopy in (A) tris–acetate, (B) tris–HCl, and (C) potassium phosphate buffers, all at pH 7.4. Profiles obtained using protein solutions without magnesium (1 mM EDTA present) are presented in dashed lines. Continuous lines correspond to the experiments performed with 2 mM $MgSO_4$. Protein concentration was 10 μg mL$^{-1}$.

### 3.2. The effect of magnesium on thermal denaturation transitions of yeast enolase

When protein solutions were complemented with $MgSO_4$ or $MgCl_2$ (2 mM), the yeast enolase thermal denaturation process occurred at higher temperatures compared to those without $MgSO_4$ or $MgCl_2$ (Fig. 1). We also observed that the transition in tris–HCl becomes more cooperative, while the possible intermediate species in phosphate buffer becomes less noticeable. It

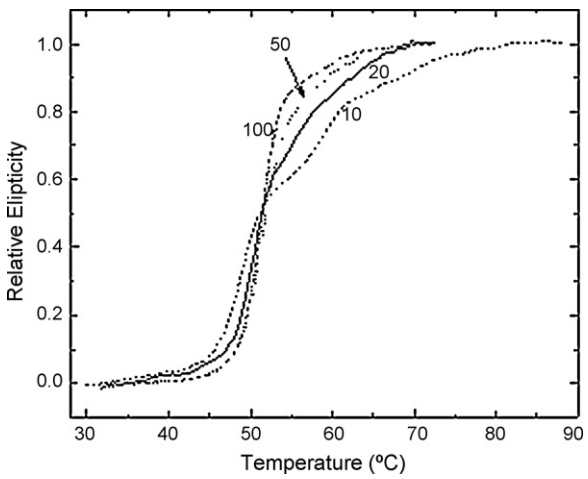


**Fig. 2.** Yeast enolase thermal denaturation curves in phosphate buffer 50 mM, at pH 7.4. The denaturation process was followed by recording ellipticity at 220 nm. Numbers indicate enolase concentrations in μg mL$^{-1}$.

is worth mentioning that the thermal stability of yeast enolase was equivalent with $MgSO_4$ or $MgCl_2$, as judged from the thermal denaturation profiles (data not shown), meaning that the observed changes in these denaturation profiles can be attributed to the presence of $Mg^{2+}$ ions alone.

### 3.3. The effect of protein concentration on the denaturation profiles

Yeast enolase denaturation curves in phosphate buffer (without $Mg^{2+}$) were measured using different protein concentrations, ranging from 10 to 100 μg mL$^{-1}$. Results of these experiments are shown in Fig. 2 (data were normalized for ease of comparison). We expected higher midpoints in the unfolding transitions of these curves with increasing protein concentration, as is commonly observed for dimeric proteins [25]. Instead, we observed denaturation profiles that began at slightly higher temperatures as the protein concentration was increased, but the unfolding profiles corresponding to higher concentrations (50 and 100 μg mL$^{-1}$) ended more sharply at lower temperatures. There are two factors contributing concomitantly to this observation. One is that cooperativity of denaturation transitions is increased with protein concentration. In addition, we observed that samples showed turbidity upon heating, almost certainly due to the aggregation of the unfolded species, which is favored when increasing the protein concentration. Therefore, we believe that aggregation might shift the completion of the unfolding reaction toward lower temperatures.

The most relevant features of these results are that a biphasic profile becomes apparent at the lowest enolase concentrations studied and that the possible intermediate becomes less noticeable at higher protein concentrations. As a general trend for dimeric proteins, a monomeric intermediate becomes more populated as protein concentrations decrease, whereas a dimeric intermediate becomes more populated as protein concentrations increase [26]. According to this, the yeast enolase thermal denaturation occurs via a three-state model, involving a monomeric intermediate that is more stable and noticeable in the presence of phosphate.

### 3.4. Reversibility of the unfolding reaction

After the completion of the thermal denaturation transitions, protein solutions were cooled down to 25 °C either at a scan speed of 4 °C min$^{-1}$ or by quickly reducing the temperature of the sample. As judged from the CD signal, the enzyme was utterly unable

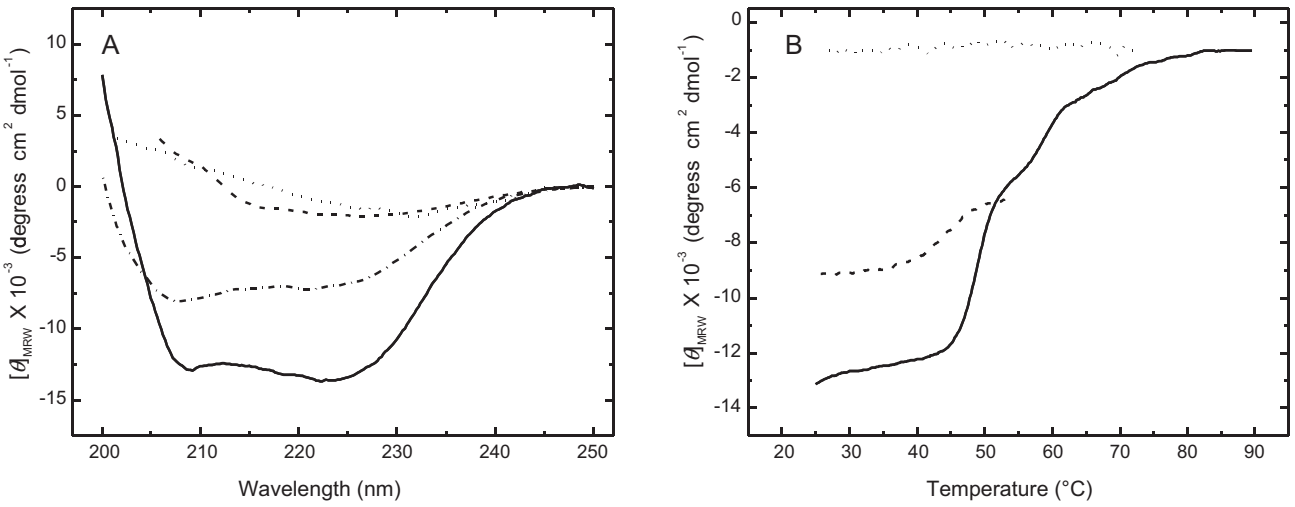


**Fig. 3.** Reversibility of the thermal denaturation of yeast enolase. (A) CD spectra of different conformations of yeast enolase. Native protein (continuous line), thermally unfolded enolase (dotted line), cooled down enolase upon thermal denaturation (dashed line), denatured protein at 55 °C for 2 min and cooled down to 25 °C (dashed and dotted line). (B) Heating and cooling profiles (4 °C $min^{-1}$). Continuous line, thermal denaturation transition; dotted line, cooling profile of yeast enolase; dashed line, cooling profile, after heat treatment at 55 °C for 2 min. Experiments were conducted in potassium phosphate buffer 50 mM, pH 7.4. Protein concentration was 10 μg $mL^{-1}$.

to refold under these experimental conditions. In other assays, the sample was heated for 1 min at 70 °C. Under this treatment, the secondary structure of the native protein disappeared as revealed by the CD signal. Immediately after heating, the sample was cooled to 25 °C at a scan speed of 4 °C $min^{-1}$, while the CD signal was monitored. These experiments revealed that the secondary structure of the native protein was not recovered, indicating that the unfolded conformation of yeast enolase is not capable of recovering its secondary structure when cooled down (Fig. 3). Commonly, irreversibility is attributed to unspecific aggregation of the denatured conformations with exposed hydrophobic surfaces. In our experiments (10 μg $mL^{-1}$ of protein concentration), aggregation was confirmed spectrophotometrically by light scattering at wavelengths higher than 300 nm (data not shown).

Furthermore, to test whether the intermediate conformation of enolase was capable of recovering its native secondary structure, the sample was diluted in phosphate buffer and heated for 2 min at 55 °C. Under these conditions, the CD signal reached the value of the intermediate species. Immediately after the sample was cooled down at 4 °C $min^{-1}$, a partial recovery of the secondary structure was observed (Fig. 3). We conclude that the intermediate species of enolase recovers about 70–75% of its secondary native structure and about 60% of its glycolytic activity (data not shown) when it is rapidly cooled down, which might indicate that irreversibility results from the aggregation of extensively unfolded species.

### 3.5. Effect of the heating rate on the denaturation profiles

Thermal scannings of the protein at different heating rates were also made using tris–acetate buffer. Fig. 4A shows the denaturation profiles obtained at 0.5, 1.0, 2.0, and 4.0 °C $min^{-1}$. It can be observed that the unfolding transition is strongly dependent on the heating rate. This is a common finding for denaturation processes that are kinetically controlled, due to the presence of an irreversible reaction [27–31]. In view of the irreversibility of the thermal denaturation transitions of yeast enolase evaluated in tris–acetate buffer and because they do not exhibit any noticeable intermediates, we first analyzed these transition-curves in terms of a two-state irreversible process represented as:

$$N_2 \xrightarrow{k} 2D \quad (1)$$

where $N_2$ is the native dimeric state, D the irreversibly unfolded monomeric state, and $k$ is a first-order kinetic constant. The transition curve is assumed to start at a temperature low enough to make the reaction rate negligible, and hence, the concentration of the native state is equal to the total protein concentration. Sánchez-Ruiz has derived a set of mathematical relations to estimate the activation energy, $E_a$, of the process [30]. One of the mathematical relationships relates the melting temperature, $T_m$, to the heating rate, $v$:

$$ln\frac{v}{T_m^2} = \ln\frac{AE_a}{R} - \frac{E_a}{RT_m} \quad (2)$$

where $A$ is the frequency or pre-exponential factor in the Arrhenius equation. The data profiles from Fig. 4A were used to construct the plot of $\ln(v/T_m^2)$ versus $1/T_m$ shown in the inset of this figure. This plot shows a curvature, suggesting that the thermal denaturation of yeast enolase without $Mg^{2+}$ might not be an elementary reaction occurring in a single step with a single transition state. Instead, it might occur through a three-state mechanism, *i.e.*, populating an intermediate conformation not stable enough to become noticeable under some conditions. The thermal scannings were repeated under similar experimental conditions, except the buffer was complemented with 2 mM $MgSO_4$. In these cases, the unfolding reaction is also strongly dependent on the heating rate (Fig. 4B), but the plot of $\ln(v/T_m^2)$ versus $1/T_m$ (inset of Fig. 4B) resulted in a straight line. These results suggest that the thermal unfolding of yeast enolase without $Mg^{2+}$ occurs through a three-state mechanism, although the intermediate species is undetectable in some of the denaturation transitions. The presence of $Mg^{2+}$ not only shifts the thermal transitions toward higher temperatures, but it also might destabilize any partially folded conformations, making any intermediate less noticeable or nonexistent. In the coming sections, these statements will be confirmed by studying the unfolding kinetics of yeast enolase.

### 3.6. Denaturation kinetics

The time course of yeast enolase denaturation at a constant temperature was examined by changes in far UV-CD at 220 nm at different temperatures in tris–acetate buffer. Fig. 5 (panel A) shows three of the kinetic curves obtained (48.2, 56.3 and 59.3 °C). In all cases, double exponential decay curves fitted well to the

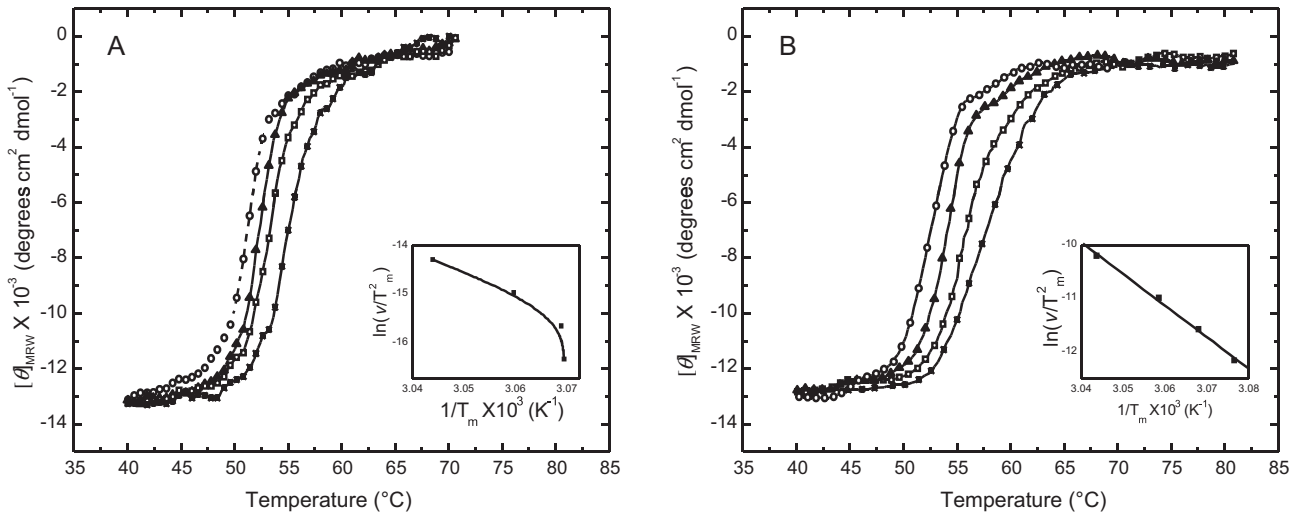


**Fig. 4.** Thermal denaturation curves of yeast enolase obtained at different heating rates: 0.5 (○), 1.0 (▲), 2.0 (□), and 4.0 (*)°C min$^{-1}$. The denaturation process was followed by recording ellipticity at 220 nm. Protein solutions were 10 μg mL$^{-1}$ in tris–acetate buffer 50 mM, pH 7.4 (without $Mg^{2+}$, Panel A and with $Mg^{2+}$, Panel B). The insets correspond to the plots of ln ($v/T_m^2$) versus $1/T_m$. Each point corresponds to one of the four transition curves shown in this figure.

experimental data. This might indicate the presence of at least one kinetic intermediate under these experimental conditions. The values of ellipticity were extrapolated to time zero and proved to be very similar to those expected for the native protein. These results indicate that if there is a fast kinetic phase (lost during the dead time of the experiments), it does not involve significant secondary-structure changes. The rate constants associated with the unfolding reaction were calculated by fitting the data.

Additional characterization of the time course of yeast enolase thermal denaturation was achieved by fluorescence experiments. Kinetic curves were constructed from the intensities of the emission measured at 340 nm. Fig. 6 shows one representative curve (56.0 °C). This plot shows an initial increment of the fluorescence emission signal, followed by a reduction in the emission intensity. A similar behavior was observed at the other temperatures. Fitting these curves to double decay equations enabled the rate constants to be calculated. In addition, emission spectra were obtained to explore the changes in fluorescence signal during the thermal unfolding of yeast enolase, using the same procedure as with the kinetic curves, but instead of continuously monitoring a single emission wavelength, spectra were recorded at a constant temperature every 3 min, immediately after the temperature jump. The inset in Fig. 6 shows spectra recorded in this way at 56.0 °C. Unfortunately, it was not possible to detect any initial increase in fluorescence emission as was observed for the kinetic curves. The simplest explanation for this behavior is that it is not possible to obtain fluorescence spectra any faster than 100 nm per 3 min with our equipment. The second emission spectra started after about 3 min and reached 340 nm about 4.2 min after the temperature jump. However, the kinetic curve from the same temperature displays a fluorescence emission increase within the first 215 s (3.58 min), with the fluorescence emission decreasing afterwards. This indicates that the first phase would not be noticeable in the time course of the second spectrum. In addition to this fluorescence intensity reduction, a red-shift to larger wavelengths of the spectra was detected, indicating an increase in the accessibility of the tryptophanyl fluorophores to solvent during the unfolding process.

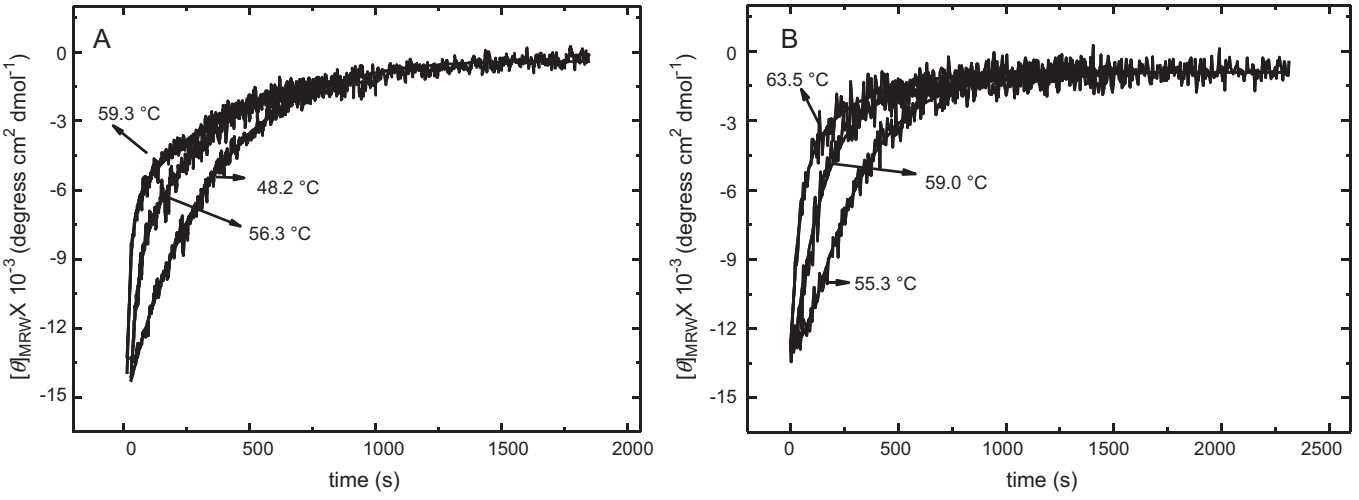


**Fig. 5.** Kinetics of the thermal denaturation of yeast enolase at different temperatures followed by CD spectroscopy at 220 nm. (A) Experiments made in tris–acetate buffer at pH 7.4. (B) Data obtained in tris–acetate buffer complemented with $MgSO_4$ 2 mM. Smooth lines are double (A) or simple (B) exponential decay curves fitted to the experimental data. Protein concentration was 10 μg mL$^{-1}$.

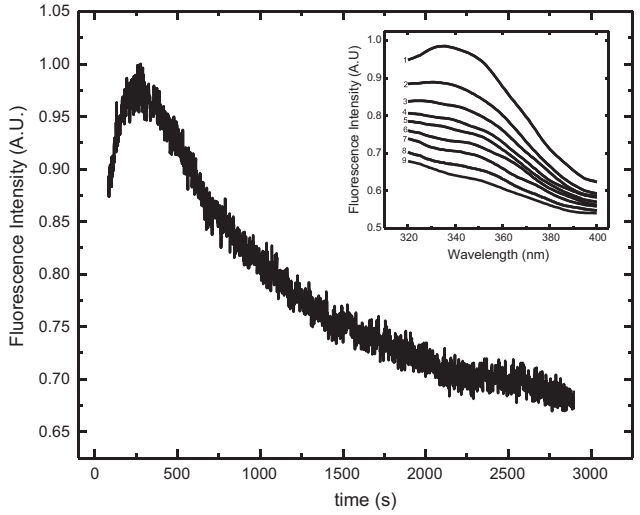


**Fig. 6.** Kinetics of the thermal denaturation of yeast enolase monitored by recording intrinsic fluorescence emission at 320 nm (excitation wavelength was 280 nm), at 56 °C. The inset shows intrinsic fluorescence emission-spectra recorded immediately after the temperature jump, at 56 °C every 3 min. Experiments were carried out in tris–acetate buffer 50 mM, at pH 7.4, and the protein concentration was 10 μg mL$^{-1}$.

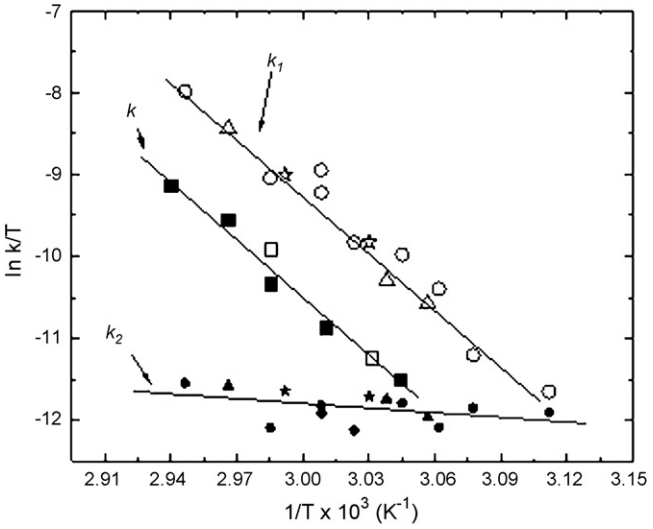


**Fig. 8.** Eyring plots for the rate constants of unfolding of yeast enolase. The data correspond to $k$, $k_1$, and $k_2$ as indicated. Denaturation data were obtained by far-UV CD ($k$: ■, $k_1$: ○ and $k_2$: ●), intrinsic fluorescence ($k$: □, $k_1$: △ and $k_2$: ▲) and ANS fluorescence ($k_1$: ☆ and $k_2$: ⋆). Lines shown are least-squares regressions according to equation 3.

### 3.7. Binding of a hydrophobic dye

The time course denaturation of yeast enolase was also explored in the presence of ANS. One representative kinetic curve obtained in tris–acetate buffer complemented with 100 μM ANS at 56.0 °C is shown in Fig. 7. First, an increase in the ANS-fluorescence emission is observed, followed by a larger decrease in signal. This observation is consistent with the formation of a molten globule-like species. Thus, the kinetic intermediate observed in the thermal denaturation of yeast enolase might be described as such a state. Molten globule-like intermediates have been observed in proteins of the enolase superfamily, such as N-succinylamino acid racemase [32], as well as many other proteins [29]

### 3.8. Effect of magnesium on yeast enolase denaturation kinetics

The time course of yeast enolase denaturation at a constant temperature was also studied in tris–acetate buffer complemented with $MgCl_2$. Fig. 5 (panel B) shows three of the kinetic curves obtained by evaluating the changes in ellipticity at 220 nm at three different temperatures (55.3, 59.0, and 63.5 °C). In this case, all kinetic curves are single exponential decay curves, in contrast to what was observed without $Mg^{2+}$. Therefore, experimental data were fitted to a single exponential equation to obtain rate constants. This behavior might indicate the absence of any detectable kinetic intermediates under these experimental conditions. Clearly, the unfolding rate constants calculated for these experimental conditions are lower than those obtained without $Mg^{2+}$ at similar temperatures, which might contribute to the commonly observed stabilizing effect of $Mg^{2+}$ on enolase [22].

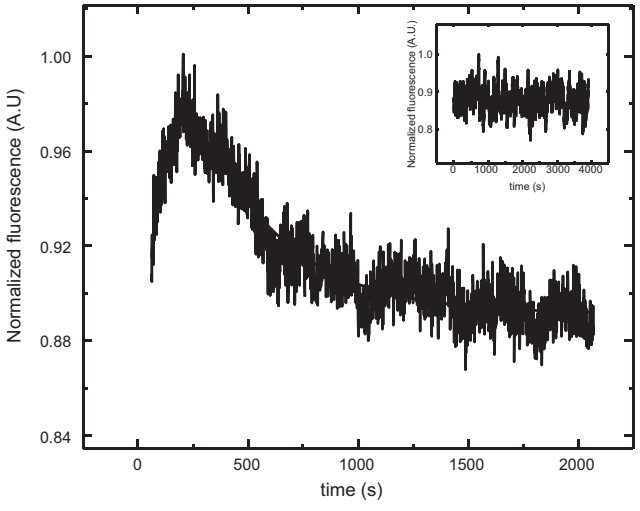


**Fig. 7.** ANS-Fluorescence emission kinetics at 56 °C. Enolase solutions were at a concentration of 10 μg mL$^{-1}$ in tris–acetate buffer complemented with ANS 100 μM. Data points were fitted to a biphasic exponential decay equation (smooth line).

### 3.9. Temperature dependence of the unfolding rate constants

The effect of temperature on the rate constants of the reaction, observed by changes in the secondary and tertiary structure during the denaturation of yeast enolase ($k$, $k_1$, and $k_2$), is illustrated in Fig. 8. The ln($k$/$T$) versus 1/$T$ plot employs Eyring's equation:

$$ln\frac{k}{T} = \ln\frac{k_B}{\hbar} + \frac{\Delta S^{\neq}}{R} - \frac{\Delta H^{\neq}}{RT} \quad (3)$$

where $k$ is the rate constant of an elementary reaction; $k_B$ and $\hbar$ are Boltzman's and Planck's constants, respectively; and $\Delta H^{\neq}$ and $\Delta S^{\neq}$ are the activation enthalpy and entropy, respectively. There are three sets of data in Fig. 8; data on the highest and lowest lines belong to the first ($k_1$) and second ($k_2$) kinetic constants from experiments without $Mg^{2+}$. Points forming the middle line are from the unique rate constants ($k$) calculated from experiments with $Mg^{2+}$. The data describe linear ln($k$/$T$) versus 1/$T$ plots. Linearity of Eyring's plot is a common finding when the variation of $\Delta H^{\neq}$ with temperature ($\Delta Cp^{\neq}$) is practically negligible ($\Delta Cp^{\neq} \approx 0$), indicating small changes in solvent accessibility to reach the transition state [27,29]. Interestingly, data from experiments with ($k$) and without ($k_1$) $Mg^{2+}$ exhibit almost identical slopes, suggesting that $\Delta H^{\neq}$ and $\Delta Cp^{\neq}$ are similar under both conditions. Fitting of unfolding data from circular dichroism, intrinsic and ANS fluorescence emission to the Eyring's equation produces the $\Delta H^{\neq}$ values shown in Table 1. Clearly, the activation enthalpy values obtained from the experiments with magnesium ($\Delta H^{\neq}$) and the first reaction observed in

**Table 1**
Activation enthalpies that characterize yeast enolase thermal unfolding.[a],[b]

| Condition | Proposed mechanism | $\Delta H^{\neq}$ (kJ mol$^{-1}$) | $\Delta H_1^{\neq}$ (kJ mol$^{-1}$) | $\Delta H_2^{\neq}$ (kJ mol$^{-1}$) |
|---|---|---|---|---|
| $-Mg^{2+}$ | $N_2 \underset{k_{-1}}{\overset{k_1}{\leftrightarrow}} 2I \overset{k_2}{\rightarrow} 2D$ | | 185 (20) | 25 (8) |
| $+Mg^{2+}$ | $N_2 \overset{k}{\rightarrow} 2D$ | 190 (30) | | |

[a] Activation parameters were calculated from the least-squares regressions of data in Fig. 8 according to Eq. (3).
[b] Standard deviations are indicated in parentheses.

experiments without the cation ($\Delta H_1^{\neq}$) are almost identical, where the difference is within the error of the measurements.

## 4. Discussion

Enolase is involved in a variety of cellular processes including glycolysis and gluconeogenesis and can act as a plasminogen receptor on the cell surface of several organisms, among other functions. Despite its multifunctionality, its stability and the folding/unfolding reaction have yet to be fully explored. Here, we report the yeast enolase thermal denaturation unfolding profile and kinetic experiments, with or without $Mg^{2+}$, its natural cofactor. Possible models of the unfolding reaction in each experimental condition are proposed.

### 4.1. Unfolding of apo-enolase occurs via a monomeric intermediate

The yeast enolase thermal denaturation profiles were obtained using far-UV CD over a wide range of experimental conditions. When using phosphate buffer and no $Mg^{2+}$ (1 mM EDTA present), the unfolding transition was shown to be biphasic with the population of an intermediate species, which became more apparent as protein concentration decreased, as expected for a monomeric intermediate [33–35]. Some studies report the ability of the phosphate group to stabilize native enzyme conformations with substrates that include a phosphate group [29]. This could be attributed to the interaction of the phosphate group with catalytic site residues. The phosphate group does not have an important effect on the stability of the native form of yeast enolase, as the unfolding temperature was not significantly modified. Instead, it mainly stabilizes a monomeric intermediate species, enough to become visible in the transition curve.

Some reports indicate that enolase is stabilized after substrate or substrate-analog binding [22]. However, we did not observe any native conformation stabilization, probably because phosphate does not bind strongly enough to enolase, as substrate or analogs do. However, the rest of the experimental conditions studied here produced highly irreversible-monophasic profiles without any noticeable intermediates. The denaturation transitions were obtained at different heating rates, and we were able to establish that the unfolding reaction of yeast enolase is kinetically controlled. Having determined the kinetic control of the process, we constructed the plots of $\ln(\nu/T_m^2)$ versus $1/T_m$ (insets of Fig. 4A and B). An elementary reaction proceeds through a single reaction step with a single transition state; therefore, we would expect a linear behavior of the plot $\ln(\nu/T_m^2)$ versus $1/T_m$.

The plot without $Mg^{2+}$ displays a large curvature (inset of Fig. 4A), indicating that the yeast enolase unfolding reaction might consist of more than one step, populating an intermediate state with more than one transition state. Kinetic experiments confirmed this, indicating that the unfolding reaction of yeast enolase without $Mg^{2+}$ happens in at least two steps. Furthermore, we were able to detect the interaction of the intermediate species with ANS. Thus, the intermediate state can be described as a monomeric molten globule-like conformation, which preserves part of its secondary structure, and the region nearby the catalytic site might be partially structured. In addition, this intermediate species recovers part of its secondary structure if immediately cooled down.

Rate-constants of each kinetic curve were calculated from kinetic experiments and were used to build the Eyring plot. It is worth mentioning that the rate constants calculated from kinetic experiments following different spectroscopic techniques are similar at the same temperatures, and their dependence on temperature is similar implying that they all correspond to the same reaction. We propose that the simplest model of protein denaturation should include two steps: reversible unfolding and dissociation and irreversible alteration of the unfolded state to produce a final denatured state, unable to fold back to the native protein. This scheme is known as the Lumry Eyring model [36]:

$$N_2 \underset{k_{-1}}{\overset{k_1}{\leftrightarrow}} 2I \overset{k_2}{\rightarrow} 2D \quad (4)$$

where $N_2$ is the native dimer, I is the monomeric molten globule-like intermediate monomer, D is the irreversibly denatured monomer, $k_1$ and $k_{-1}$ are the rate constants for the forward and reverse unfolding process with concomitant dissociation, and $k_2$ is the rate constant for the denaturation of the monomers.

### 4.2. The effect of magnesium on the denaturation mechanism of yeast enolase

In general, di- and trivalent cations, such as $Mg^{2+}$, $Mn^{2+}$, $Ca^{2+}$ and $Tb^{3+}$, among others, stabilize enolase by reducing subunit dissociation [15,22,23,37–41]. However, there are several ways to increase the overall stability of the native state. For example, metal binding could decrease the value of the equilibrium constant of denaturation or increase the rate constant of renaturation. Alternatively, metal binding could also stabilize the native state by reducing the rate constant of denaturation. All these possibilities or a combination of them would favor the native state. In our case, we were not able to find reversibility of the denatured state; therefore, we could not calculate the rate constant of renaturation or the equilibrium constant. However, our results indicate that the unfolding rate-constants are smaller when $Mg^{2+}$ is present in the protein solution, which means that the unfolding reaction occurs much more slowly with $Mg^{2+}$, thus favoring the native state.

In addition, the presence of $Mg^{2+}$ modifies the folding pathway of yeast enolase. With $Mg^{2+}$, the monomeric intermediate species becomes less noticeable or even nonexistent. There are several experimental findings supporting this statement: first, the denaturation transitions obtained in the presence of $Mg^{2+}$ did not show any intermediate species; and second, the plot of $\ln(\nu/T_m^2)$ versus $1/T_m$ (inset of Fig. 4B) resulted in a straight line, as expected for an elementary reaction proceeding through a single reaction step with a single transition state. Further evidence of a single step reaction was obtained from monophasic kinetic curves. Therefore, in this case, an irreversible two-state model is more suitable to describe the denaturation of yeast enolase:

$$N_2 \overset{k}{\rightarrow} 2D \quad (5)$$

## 5. Conclusions

Previous studies of enolase thermal denaturation have suggested that this multifunctional protein might follow different folding/unfolding mechanisms, with or without $Mg^{2+}$ [22] but with similar calorimetric enthalpy changes. Here, we detected different mechanisms, with similar activation enthalpies. These results improve our understanding of the thermal unfolding of yeast enolase and its stabilization by $Mg^{2+}$.

The effects of a variety of metallic and nonmetallic cofactors on the folding/unfolding pathways of several enzymes have been reported. In most cases, cofactors stabilize their corresponding proteins, but they usually do not perturb folding mechanisms, suggesting that cofactors mainly bind to native proteins. In the case of enolase, binding of $Mg^{2+}$ modifies the unfolding pathway.

## Acknowledgements

This work was supported by grants from TWAS, CONACyT (45990 and 101229), ICyT-DF (6968), and SIP-IPN (20111186).

## References

[1] H. Iida, I. Yahara, J. Cell Biol. 99 (1984) 1441–1450.
[2] L.A. Miles, C.M. Dahlberg, J. Plescia, J. Felez, K. Kato, E.F. Plow, Biochemistry 30 (1991) 1682–1691.
[3] A. Redlitz, B.J. Fowler, E.F. Plow, L.A. Miles, Eur. J. Biochem. 227 (1995) 407–415.
[4] V. Pancholi, Cell. Mol. Life Sci. 58 (2001) 902–920.
[5] J. Petrak, R. Ivanek, O. Toman, R. Cmejla, J. Cmejlova, D. Vyoral, Proteomics 8 (2008) 1744–1749.
[6] L.D. Faller, A.M. Johnson, Proc. Natl. Acad. Sci. U. S. A. 71 (1974) 1083–1087.
[7] E. Zhang, J.M. Brewer, W. Minor, L.A. Carreira, L. Lebioda, Biochemistry 36 (1997) 12526–12534.
[8] J.M. Brewer, CRC Crit. Rev. Biochem. 11 (1981) 209–254.
[9] J.M. Brewer, C.V.C. Glover, M.J. Holland, L. Lebioda, J. Protein Chem. 22 (2003) 353–361.
[10] T.M. Larsen, J.E. Wedekind, I. Rayment, G.H. Reed, Biochemistry 35 (1996) 4349–4358.
[11] L. Lebioda, B. Stec, J.M. Brewer, J. Biol. Chem. 264 (1989) 3685–3693.
[12] L. Lebioda, E. Zhang, K. Lewinski, J.M. Brewer, Proteins 16 (1993) 219–225.
[13] R.R. Poyner, T.M. Larsen, S. Wong, G.H. Reed, Arch. Biochem. Biophys. 401 (2002) 155–163.
[14] J.E. Wedekind, R.R. Poyner, G.H. Reed, I. Rayment, Biochemistry 33 (1994) 9333–9342.
[15] S. Zhao, B.S.F. Choy, M.J. Kornblatt, FEBS J. 275 (2008) 97–106.
[16] J.M. Brewer, J.S. McKinnon, R.S. Phillips, FEBS Lett. 584 (2010) 979–983.
[17] V. Hannaert, M. Albert, D.J. Rigden, M.T. da Silva Giotto, O. Thiemann, R.C. Garratt, Eur. J. Biochem. 270 (2003) 3205–3213.
[18] T. Hosaka, T. Meguro, I. Yamato, Y. Shirakihara, J. Biochem. 133 (2003) 817–823.
[19] H.J. Kang, S. Jung, S.J. Kim, S.J. Chung, Acta Crystallogr. D: Biol. Crystallogr. 64 (2008) 651–657.
[20] J. Qin, G. Chai, J.M. Brewer, L. Lovelace, L. Lebioda, Biochemistry 45 (2006) 793–800.
[21] W.H. Holleman, Biochim. Biophys. Acta 327 (1973) 176–185.
[22] J.M. Brewer, J.E. Wampler, Int. J. Biol. Macromol. 28 (2001) 213–218.
[23] J.M. Brewer, C.V. Glover, M.J. Holland, L. Lebioda, Biochim. Biophys. Acta 1340 (1997) 88–96.
[24] D.S. Sánchez-Miguel, J. Romero-Jiménez, C.A. Reyes-López, A.L. Cabrera-Avila, N. Carrillo-Ibarra, C.G. Benítez-Cardoza, Protein J. 29 (2010) 1–10.
[25] K.E. Neet, D.E. Timm, Protein Sci. 3 (1994) 2167–2174.
[26] J.A. Rumfeldt, C. Galvagnion, K.A. Vassall, E.M. Meiering, Prog. Biophys. Mol. Biol. 98 (2008) 61–84.
[27] C.G. Benítez-Cardoza, A. Rojo-Domínguez, A. Hernández-Arana, Biochemistry 40 (2001) 9049–9058.
[28] E. Freire, W.W. van Osdol, O.L. Mayorga, J.M. Sanchez-Ruiz, Annu Rev Biophys Biophys Chem. 19 (1990) 159–188.
[29] E. Mixcoha-Hernández, L.M. Moreno-Vargas, A. Rojo-Domínguez, C.G. Benítez-Cardoza, Protein J. 26 (2007) 491–498.
[30] J.M. Sánchez-Ruiz, Biophys. J. 61 (1992) 921–935.
[31] S.R. Tello-Solis, A. Hernández-Arana, Biochem. J. 311 (1995) 969–974.
[32] J. Pozo-Dengra, S. Martínez-Rodríguez, L.M. Contreras, J. Prieto, M. Andújar-Sánchez, J.M. Clemente-Jiménez, Biopolymers 91 (2009) 757–772.
[33] S.A. Hobart, S. Ilin, D.F. Moriarty, R. Osuna, W. Colón, Protein Sci. 11 (2002) 1671–1680.
[34] A.L. Mallam, S.E. Jackson, J. Mol. Biol. 359 (2006) 1420–1436.
[35] Y.C. Park, H. Bedouelle, J. Biol. Chem. 273 (1998) 18052–18059.
[36] L.S. Zamorano, D.G. Pina, J.B. Arellano, S.A. Bursakov, A.P. Zhadan, J.J. Calvete, Biochimie 90 (2008) 1737–1749.
[37] T.H. Gawronski, E.W. Westhead, Biochemistry 8 (1969) 4261–4270.
[38] M.J. Kornblatt, A. Al-Ghanim, J.A. Kornblatt, Eur. J. Biochem. 236 (1996) 78–84.
[39] M.J. Kornblatt, R. Lange, C. Balny, Eur. J. Biochem. 271 (2004) 3897–3904.
[40] A. Rosenberg, R. Lumry, Biochemistry 3 (1964) 1055–1061.
[41] E.W. Westhead, Biochemistry 3 (1964) 1062–1068.
[42] C.C. Chin, J.M. Brewer, F. Wold, J. Biol. Chem. 256 (1981) 1377–1384.